*Economic Geology*
Vol. 95, 2000, pp. 391–404

# Gold-Bearing Breccias of the Rain Mine, Carlin Trend, Nevada

Cindy L. Williams,

*Newmont Mining Company, 1700 Lincoln St., Denver, Colorado 80203*

Tommy B. Thompson,[†]

*Center for Research in Economic Geology (CREG), Mackay School of Mines/169, University of Nevada, Reno, Nevada 89557-0232*

Jon. L. Powell, and W. Warren Dunbar

*Newmont Mining Company, P.O. Box 669, Carlin, Nevada 89822*

## Abstract

The Rain mine includes two mined-out open pits that contained 36.4 t (1.17 Moz) gold, averaging 1.8 g/t gold, and underground reserves, including underground production, estimated at 4.9 t (157,000 oz) gold averaging 7.7 g/t. Rain orebodies are localized in a breccia complex within the hanging wall of the Rain fault and hosted within the Mississippian Webb Formation immediately overlying the contact with the Devonian Devils Gate Limestone.

The ore host includes four texturally and genetically distinct breccia types: (1) crackle breccia; (2) hydrothermal breccia; (3) tuffisite with accretionary lapilli; and (4) collapse breccia. Crackle breccia forms a capping over multistage hydrothermal breccias that are cut by tabular- to pipe-shaped tuffisite dikes, with some containing accretionary lapilli. Pre- and synore hydrothermal breccias formed during at least three episodes of convective fluidization, followed by quartz-sulfide-barite cementation. High-grade gold was deposited as a late phase along the upper portion of the hydrothermal breccia mass and extended into the crackle breccia zone. Collapse breccias occur along the floor of the composite breccia mass and have irregular upper and lower contacts. The lower contact occurs on a dissolution boundary with the Devils Gate Limestone.

Matrix-supported, heterolithic, hydrothermal breccias at Rain consist of sedimentary rock fragments composed of sandstone, siltstone, mudstone, limestone, and conglomerate. Some fragments contain as much as 8 percent introduced biotite in veinlets and/or fragment matrix replacements. The veinlets consist of euhedral quartz, biotite, sphalerite, and pyrite. Barite constitutes as much as 60 percent of the hydrothermal breccias in the form of fragments and as a cement to the breccias. Quartz replacement of fragments and as a breccia cement is pervasive. The total sulfide content in unoxidized ores is less than 5 volume percent.

The Rain orebody resulted from five interpreted stages of development: (1) structural preparation along the right-lateral oblique Rain fault system and conjugate left-lateral oblique northeast-striking faults; (2) multiple episodes of hydrothermal breccia formation, with high-grade gold deposition immediately following the last brecciation event; (3) late channelized and fluidized rock fragments and fine clays forming tuffisite bodies with accretionary lapilli; (4) postmineral extensional reactivation of structures; and (5) collapse brecciation resulting from postore supergene acidic fluid ponding on and dissolving the upper Devils Gate Limestone.

The age of the Rain orebody is poorly constrained. It is older than 22 Ma supergene alunite, but no maximum age constraints other than the Mississippian host rock are known.

## Introduction

The Rain mine on the southern Carlin trend is 29 km south of Carlin in Elko County, Nevada (Fig. 1). The Rain mineralized system includes, from southeast to northwest, small oxide gold inventories at Emigrant, Snow Peak, BJ Hill, and Gnome, the mined-out Rain and Southern mineralized zone pits, the Rain underground mine, and underground inventories including northwest Rain and Tess. The Rain deposit is unique, compared to other Carlin-type gold deposits, in that it is hosted by a hydrothermal breccia mass that extends at least 5 km along the Rain fault.

This paper is based on: (1) current observations and interpretations by Newmont Mining Co. mine and exploration geologists; (2) 1997 field and lab work (T.B. Thompson); (3) observations from previously involved Newmont geologists; and (4) a master's thesis (Williams, 1992). Reported here are field relationships including stratigraphy, structural geology, breccia body geometry, and textures, and interpreted origins and gold orebody geometry.

[†]Corresponding author: email, tommyt@mines.unr.edu

## History and Gold Endowment

The Rain deposit was discovered in 1980 by P. Montrose, who submitted it to Newmont (Knutsen and West, 1984). The discovery outcrop was a jasperoid ridge along the Rain fault. The jasperoid contained massive barite, alunite, and gold values up to 17 ppm (Knutsen and West, 1984). By 1987, an open pit minable reserve of 22.5 Mt at 1.8 g/t gold or 1.17 Moz was defined. Open pit mining was conducted between 1987 and 1994. The Rain deposit extended to the northwest from the open pit, but it was too small to support the high stripping ratio required for open pit mining. It was evaluated as a potential underground operation and in October, 1993, two portals collared in the northwest Rain pit highwall began the Carlin trend's first underground mine. Ultimately, the

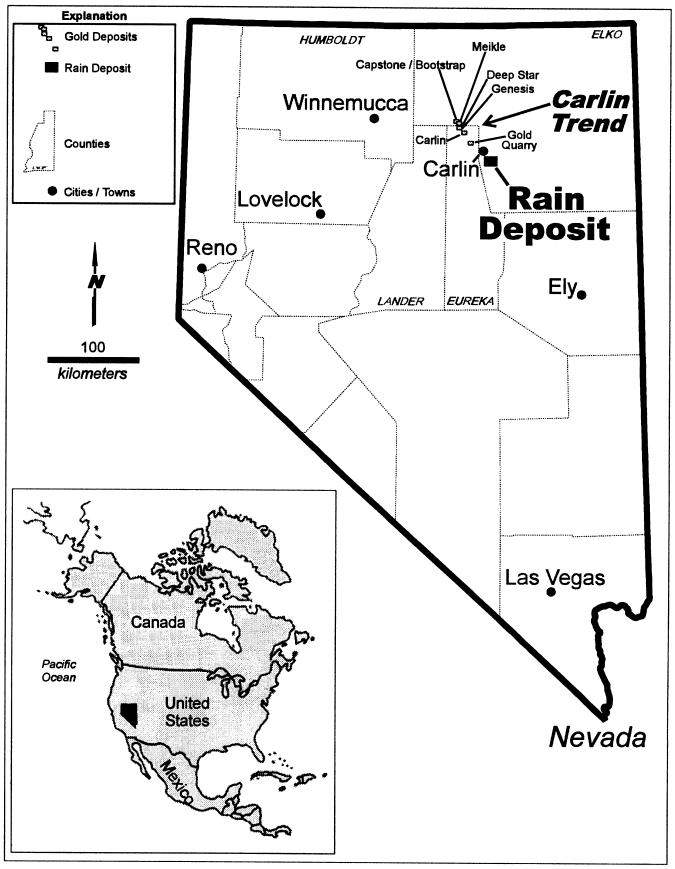


FIG. 1. Index map of the Carlin trend with location of the Rain deposit at the southern end of the trend.

resource was discovered to extend much further to the northwest and by January, 1996 the reported oxide reserves plus production totaled 157,150 oz Au, averaging 7.7 g/t. The underground reserve is currently divided into four areas: stopes 1 and 2 and zones 3 and 4 (Figs. 2 and 3). The stopes and zones nomenclature was established on the basis of the fault-bounded ore blocks shown on Figures 2 and 3.

## Regional Geology

The Rain mine is on the Carlin trend, a 60-km-long alignment of sedimentary rock-hosted gold deposits trending north-northwest across northeastern Nevada (Fig. 1). Past gold production, reserves, and resources on the Carlin trend currently total 107 million troy oz (Teal and Jackson, 1997). The regional geology of the Carlin trend was documented by Christensen (1993) and Teal and Jackson (1997) and will only be summarized here.

During the Paleozoic era, northeastern Nevada was located along the stable western North American continental margin. Western eugeoclinal and eastern miogeoclinal sediments were deposited as interfingering packages on the continental shelf and slope. During the Late Devonian to Early Mississippian Antler orogeny, western facies siliceous rocks were placed over eastern facies carbonates along the Roberts Mountains thrust (Smith and Ketner, 1968). Fine- to coarse-grained siliceous sedimentary rocks that were eroded from the emerging highland formed the Middle Mississippian to Early Pennsylvanian overlap assemblages (Smith and Ketner, 1975) that host the Rain ores.

Subsequent compressional tectonic events from late Paleozoic (Humboldt orogeny) through Mesozoic (Sonoma and Sevier orogenies) times resulted in further complex uplift, folding, and thrusting (Stewart, 1980). Igneous events were documented as Late Jurassic (158 Ma Goldstrike stock) and late to early Oligocene (35–40 Ma dikes and sills) in age by Smith and Ketner (1975), Arehart et al. (1993), and Emsbo et al. (1996). Basin and Range extension started at 20 Ma in the area immediately northwest of Carlin (Fig. 1; Evans, 1980); however, there is not precise age control on the inception of Basin and Range extension at Rain. Early compressional events followed by Basin and Range extension and erosion created windows of eastern facies carbonate rock through the siliceous upper plate rocks. All currently known Carlin trend gold deposits occur within, or proximal to, these lower plate carbonate windows (Teal and Jackson, 1997). Although the Rain deposit is located in a lower plate window, it differs from other Carlin trend deposits because it is hosted in rocks of the Mississippian overlap assemblage, rather than in lower plate Siluro-Devonian carbonate rocks.

## Rain District Rock Units

The oldest unit exposed in the Rain mine area is the Devonian Devils Gate Limestone, an autochthonous lower plate unit that is 150 to 200 m thick. The unit is a medium- to thick-bedded micritic limestone with local stromatoporoid colonies, horn corals, and fossil hash.

The Mississippian Webb Formation of the overlap assemblage unconformably overlies the Devonian Devils Gate Limestone. The limestone surface was exposed to erosion, and karst features developed regionally prior to deposition of the Webb Formation. A terra rossa clay is common at the contact. Anomalous gold values and relatively small (<31 t) gold deposits are also common at that boundary throughout the eastern Great Basin (Maher, 1997).

The Webb Formation, 120 to 150 m thick, includes thinly bedded mudstones and siltstones with local channel sand and conglomerate lenses in the upper part. The fine-grained rocks are carbonaceous and locally exhibit turbidite graded bedding and soft-sediment deformation. The Webb Formation hosts a breccia mass that is the ore host in the Rain mine area.

The Webb Formation coarsens upward through a gradational contact with the Mississippian Chainman Formation, consisting of medium- to coarse-grained sandstone and local conglomerate. The Chainman Formation is 400 to 500 m thick and also coarsens upward. Rocks of the Webb and Chainman formations span depositional environments from preorogenic deep-water sedimentation to early orogenic overlap assemblages.

The allochthonous Devonian Woodruff Formation structurally overlies the sedimentary rocks of the eastern and overlap assemblages. The unit includes thinly bedded siltstone and mudstone with diagnostic phosphate nodules. The rocks are pervasively folded and internally deformed. The formation ranges from 90 to 350 m thick.

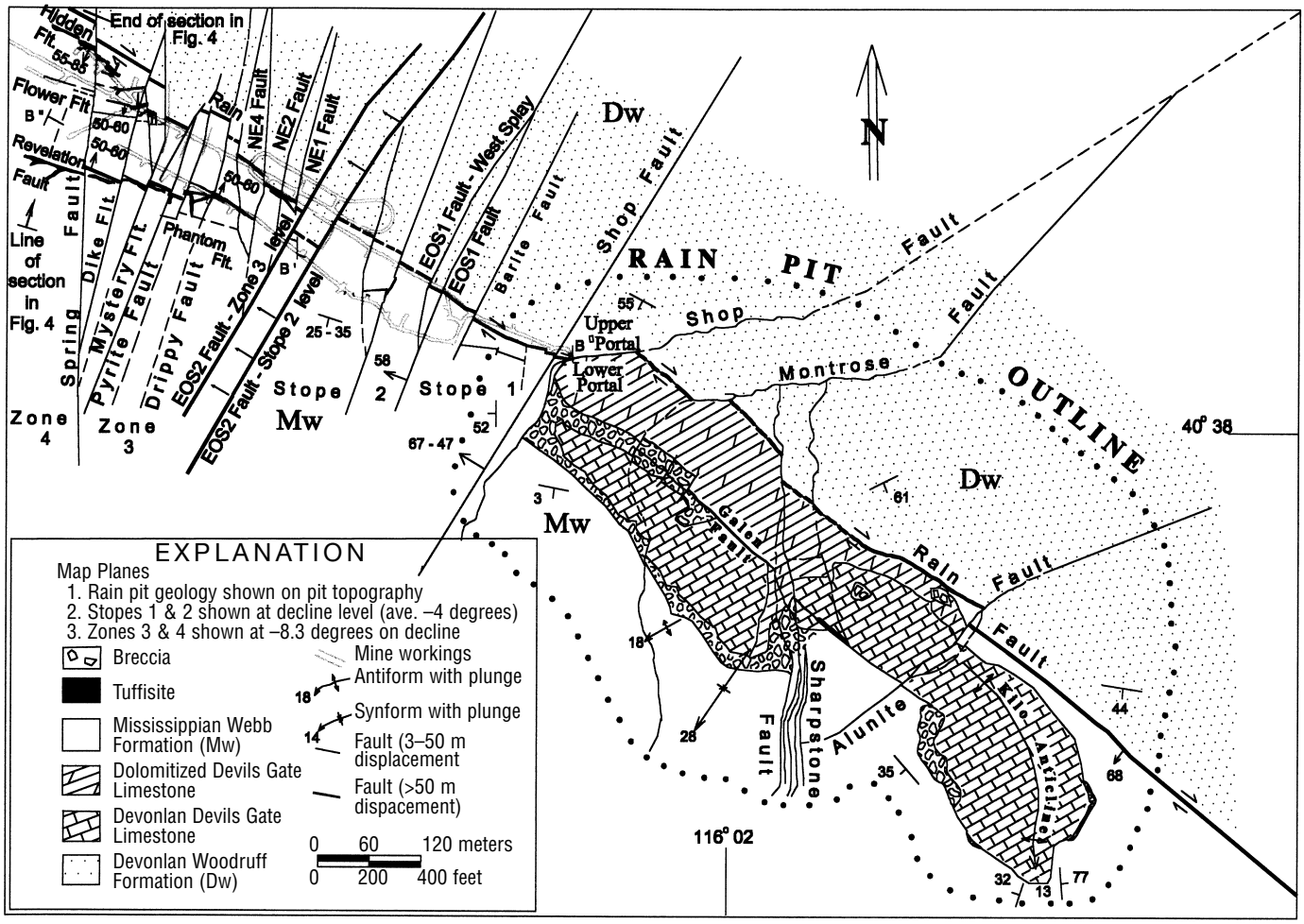


FIG. 2. Generalized geologic map extending from the Rain open pit to the northwest along the underground workings. The geology northwest of the pit is shown on the inclined plane (average dip 6° northwest) of the underground workings. The locations of cross sections in Figure 3 (B-B'-B") and Figure 4 are indicated.

## Structural Geology

### *Introduction*

Two fault sets dominate the structural geology of the Rain area: the northwest-striking Rain fault system, and a northeast-striking fault set (Figs. 2 and 3). The Rain fault system strikes N 40° to 50° W in the open pit but shifts more westerly in the underground exposures (N 65°–85° W), and the northeast set strikes N 0° to 45° E (Fig. 2). The Rain fault dips 68° to 80° SW in the open pit, but in the underground exposures to the northwest it flattens to 38° W. The northeast-striking faults generally dip 45° to 78° northwesterly. Observed slickenlines on the Rain fault in the open pit rake 17° to 30° S.

### *Rain fault system*

The Rain fault is the district's dominant structure in terms of offset and proximity to ore (Fig. 2) and it is traceable for more than 11 km. The fault places barren Woodruff Formation rocks in the footwall against the Webb Formation-Devils Gate Limestone contact in the hanging wall with at least 625 m of apparent reverse displacement. At ore levels, the Rain fault occurs as less than 3 cm of crushed rock separating barren Woodruff rocks from ore-bearing breccias.

En echelon subparallel faults have been recognized in the Rain pit, and recent underground exposures have uncovered more and provided information on their significance. These faults include the Galen, in the Rain pit, and the Revelation, Flower, Phantom, and Hidden, in underground zones 3 and 4. These faults, striking N 75° to 85° W, diverge 10° to 20° from the Rain fault and occur as nonconnected en echelon segments commonly less than 470 m long. The Flower, Galen, and Hidden faults dip 55° to 85° SW, subparallel to the Rain fault, whereas the Phantom and Revelation faults dip 50° to 60° NE toward the Rain fault. In zones 3 and 4, the resultant geometry is a series of uplifted and outward-flaring blocks (Fig. 4) forming a classic positive flower structure (Wilcox et al., 1973).

Exposures of the Rain subparallel faults in zones 3 and 4 are subtle; the aptly named Phantom fault is expressed as a set of fractures each less than 2 cm wide, forming a 2-m-wide zone. Displacement of the Devils Gate Limestone-Webb Formation contact is less than 6 m, and postore offset is indeterminate due to contrasting ore thickness across the fault

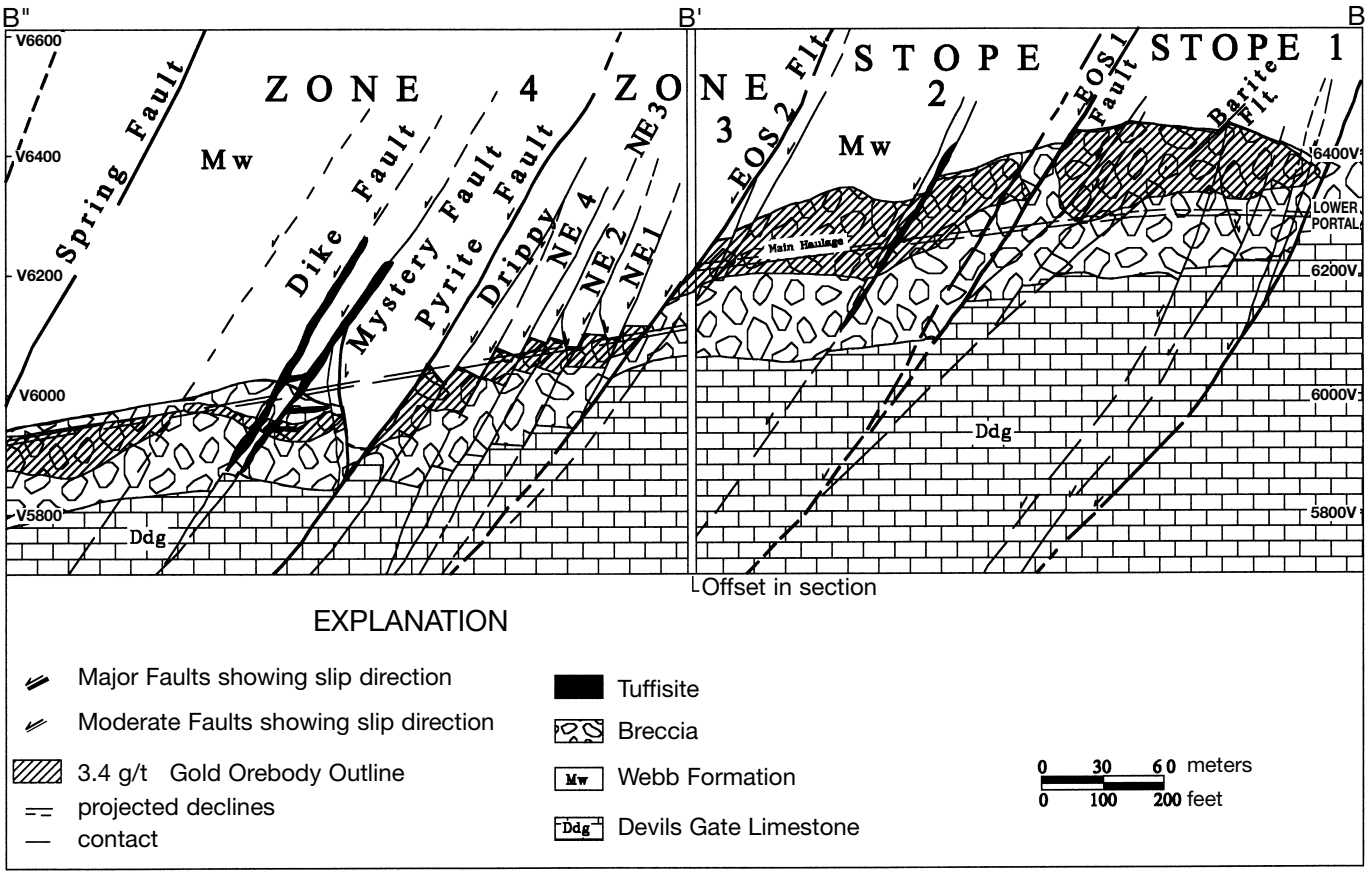


FIG. 3. Longitudinal geologic cross section B-B'-B" of Rain underground workings showing rock units, including the composite breccia mass and the gold orebody. Location of cross section is shown on Figure 2.

(Figs. 4 and 5). Despite obscure exposures, the Phantom fault juxtaposes 17.1 g/t gold-bearing breccia with visually identical but virtually barren breccia. The Revelation fault is a 15- to 35-m-wide weakly argillized zone with minor southwest- and northeast-dipping shears and anastomosing tuffisite dikes and sills (see below for description of tuffisites) that range from several centimeters to 5 m wide. The zone dips toward the Rain fault and has 15 m of apparent reverse offset of the Devils Gate Limestone surface. Orebody offset is uncertain because ore is thin or absent in the hanging wall and more than 30 m thick in the footwall. The Flower fault dips southwest with the Rain fault and exhibits apparent reverse displacement of 18 m of the Devils Gate Limestone-Webb Formation contact, but only 6 m of normal offset on the gold-bearing body.

Attempts at palinspastic restoration of the Rain fault set in two-dimensional cross sections reveal problems with volume loss and gain. These problems cannot be rectified without moving material in and out of the section plane. Such space problems can be accommodated using a strike-slip displacement interpretation (Sylvester, 1988).

Folds provide additional information on the history of the Rain fault. In the Rain pit, the asymmetric Kilo anticline occurs in the hanging wall of the Rain fault (Fig. 2). The fold axis diverges from the Rain fault in the southernmost exposures. Other folds in the hanging wall rocks are broad open folds trending southwest with shallow plunges (Figs. 2 and 6A). In contrast, the footwall rocks are tightly folded (Fig. 6B) into south-plunging asymmetrical folds at considerable distances from the Rain fault, and fold axes are oriented perpendicular to the Antler-related principal stress field (Stewart, 1980). The consistent southward plunge suggests that the footwall block has been rotated after the folds formed. In close proximity to the Rain or subparallel faults, the folds have been rotated to southwest- or west-southwest orientations consistent with drag associated with right-lateral separation. Smith and Ketner (1968) have mapped steeply dipping Eocene rocks just 2 km southeast of the Rain deposit that are folded into a southward-plunging syncline with dips as much as 70° E on the west limb, indicating post-Eocene folding. These dips in younger rocks suggest that the Paleozoic rocks along the Rain fault hanging wall may have been more steeply inclined prior to the Eocene.

While the age of original displacement on the Rain fault is unknown, lamprophyre dikes, localized along the fault northwest of the mine, area have been dated as Jurassic in age in the northern Carlin trend. The fault appears to be pre-Jurassic from those relationships.

*Northeast fault set*

The northeast fault set strikes N 0° to 45° E (Fig. 2), dipping 50° to 60° NW with 3 to 60 m of apparent normal displacement. Antithetic structures dipping 50° to 85° SE with 2

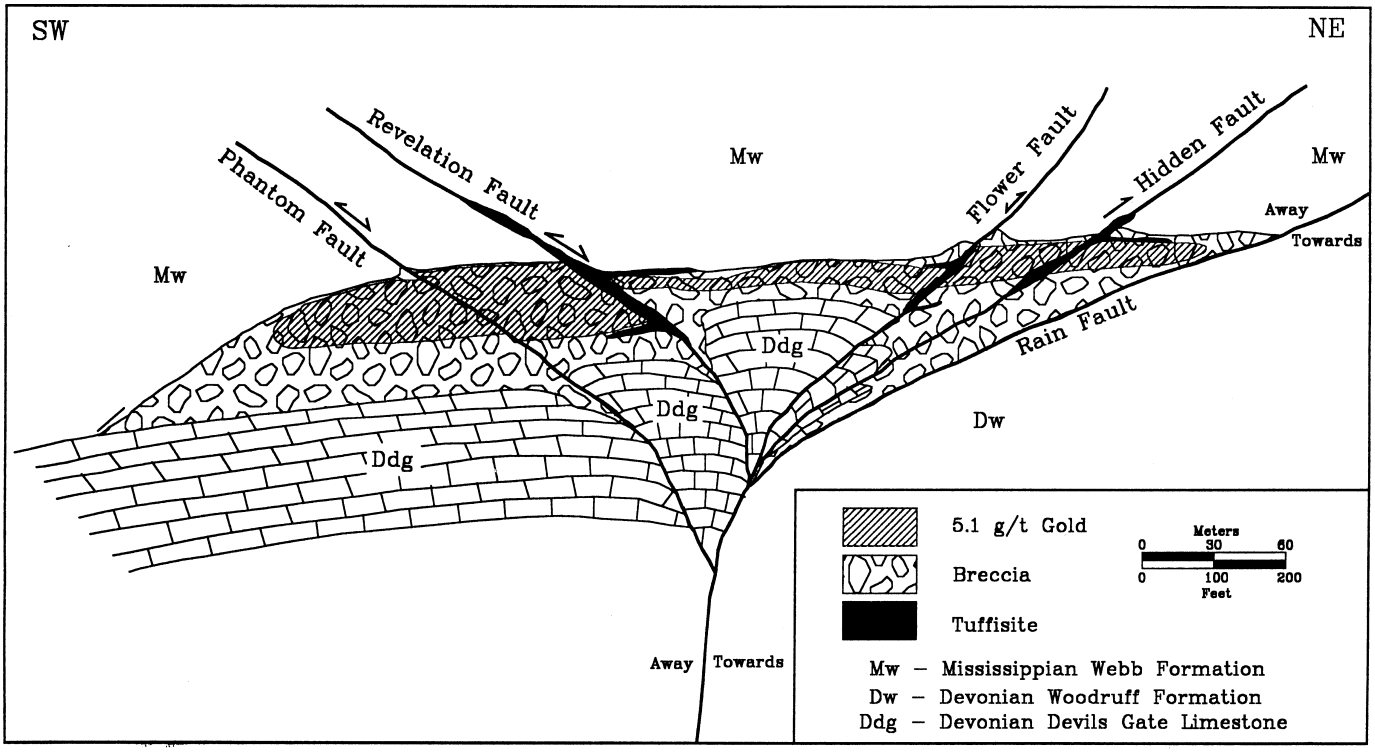


FIG. 4. Structural cross section showing zone 4 flower structure, hydrothermal breccia, and the gold orebody. Location of cross section is shown on Figure 2. Double-pronged arrows indicate faults that underwent early transpressional offset followed by extensional displacement.

to 15 m offsets are also present, but less common (Fig. 3). Fault spacings are less than 16 m, and faults exhibit listric geometries and rotation of offset blocks. The faults anastomose, especially in the brittle silicified ore horizon, forming rhombohedral blocks. Changes in fault dips range as much as 60° over 15 m of strike, and structures locally roll from northwest to southeast dips even at the underground rib scale (4 vertical m).

Near the Rain and its subparallel faults, northeast fault geometries are even more complex. Anastomosing northeast-striking faults may be spaced every 3 m, and dramatic strike and dip changes occur over short distances. The northeast-striking structures consistently offset the Rain fault. However, Rain subparallel faults may offset the northeast set, or offsets between the two may alternate with Rain subparallel faults offsetting the northeast set and, in turn, being offset by other northeast faults.

The northeast fault set can be divided into two groups: one clearly influencing gold deposition as well as offsetting ore, and the other clearly postore, i.e. offsetting the orebody and rock units. Approximately 20 percent of the northeast-striking faults controlled and localized breccia development and subsequent gold introduction (Fig. 5). These faults have a strike of N 0° to 20° E. For example, a strong ore grade and thickness enrichment occurs in the football of the Pyrite fault. In the Rain pit, breccia formation was clearly intensified along the Sharpstone fault, which shows sharply enhanced ore grade and thickness in its hanging wall. Some northeast-striking faults also form breaks where ore is shifted laterally across the fault. For example, gold ore occurs along a Rain subparallel fault in the footwall of the Shop fault, although it lies against the Rain fault in its hanging wall (Fig. 5). The remaining 80 percent of the northeast structures had no influence on gold distribution, have strikes of N 20°–45° E, and appear to have formed later during an extensional event. Most, if not all, of the earlier ore-controlling faults were reactivated by this later event.

*Controls on the Rain orebody*

The geometry and grades of gold concentrations closely parallel the Rain and earlier northeast faults (Fig. 5). The Rain fault zone is generally low grade, but the subparallel faults (e.g., the Galen fault in the Rain pit) are closely associated with high-grade zones as well as breccia masses. The orebody widens (by as much as six times) within the zone 4 area, where Rain subparallel faults (e.g., Revelation and Flower faults; Fig. 5) are developed. Similarly, the northeast-trending faults (e.g., Montrose, Barite, and Mystery faults; Fig. 5) localized sharp grade changes in the ore zone. Similar boundaries are apparent in grade-thickness maps of the Rain orebody.

*Structural interpretations*

Mutually offsetting and complex intersections between the Rain fault system and ore-controlling northeast-striking faults and their mutual true angular separations of 60° to 75° suggest reactivation of an earlier set that formed as a conjugate set to the Rain fault. Fault geometries, flower structures, fold orientations, and kinematic indicators provide strong evidence for formation in a right-lateral transpressional environment as

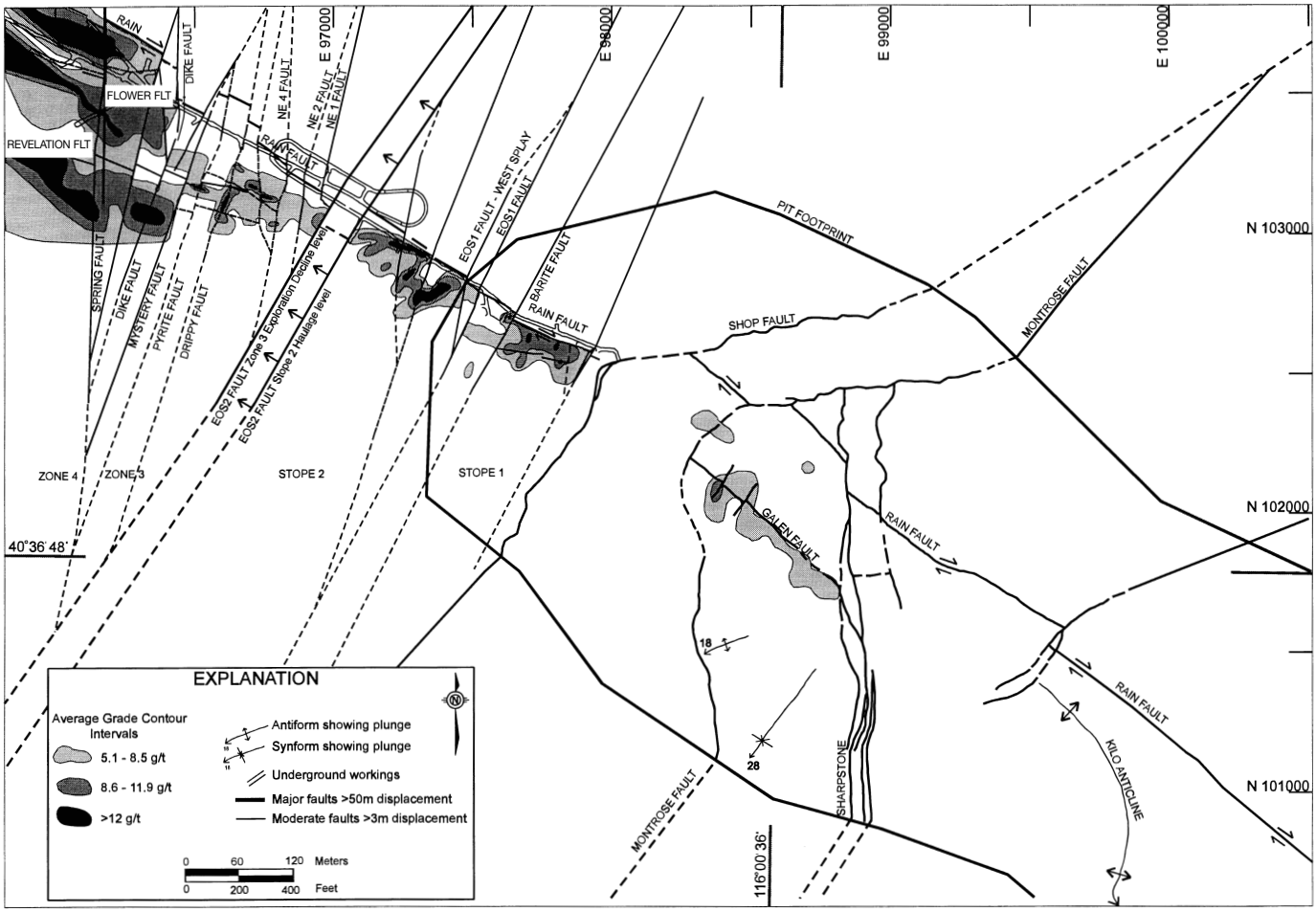


FIG. 5. Map showing average grade of gold in the Rain pit and in underground workings (stopes 1 and 2, zones 3 and 4).

defined by Sylvester (1988). Fault geometries in the Rain subdistrict are similar to simple-shear models for strike-slip fault systems (Sylvester, 1988; Fig. 6C–D). The angular separations of 60° to 75° match predictions by Sylvester's (1988) model for conjugate or antithetic shears.

Stereonet analyses indicate the average Flower fault attitude lies at a true angular separation of 14° from the average Rain fault orientation. The geometry suggests that it may have formed as a synthetic or Riedel shear (Hodgson, 1989) during Rain fault oblique-slip motion. If so, a stereonet solution indicates a 13°, S 51° E slip-line direction, or right-lateral reverse oblique displacement on the Rain fault (Fig. 6D). Similarly, the Rain and Revelation faults' slip-line solution is 3°, S 58° E. Similar stereonet analyses for the Rain open pit area yield rake solutions on the Rain fault of 25° to 35°, S 51°–56° E, or right-lateral reverse oblique slip (Fig. 6C). The average Rain fault attitude and average orientations of 50 northeast-striking fault planes (type examples of ore-controlling northeast structures) are at a true angular separation of 63°, suggesting conjugate symmetry (Fig. 6D). Notably similar to the Rain and Rain subparallel fault solutions, the predicted slip-line direction for the Rain fault with the average northeast fault data is 10°, S 48° E, again indicating dominantly strike-slip movement. Within the open pit area, the northeast-striking faults, when compared to the average Rain fault attitude, yield slip-line directions of 12° to 15°, N 27° to 48° E, suggesting left-lateral separation on the northeast faults (Fig. 6C). Most observed rakes range between 16° and 66° NE.

Strong support for a strike-slip component to Rain fault displacement is the presence of a flower structure in the Rain underground zone 4. Transpression or converging strike slip on a fault bend (Fig. 6E) provides a component of horizontal shortening, forcing compensatory uplift. The result is a series of slabs that rise upward and outward on convex-up faults over the adjacent blocks like stacked imbricate thrusts (Sylvester, 1988). This arrangement was first termed a positive flower structure by Wilcox et al. (1973).

In addition, assuming the ore-controlling northeast-striking faults and the Rain fault formed as a conjugate set, stereonet analysis indicates a principal stress direction ($\sigma_1$) of 0° to 10°, S 7° W, an orientation that would yield a significant right-lateral component of displacement on the Rain fault set and left-lateral strike-slip motion on the antithetic conjugate northeast-striking set (Fig. 6C-E). Finally, slickenlines on both fault sets locally show low-angle slip directions consistent with the projected stereonet solutions. Thrust fault orientations in the Rain footwall rocks indicate south-directed compression based on south-vergent fold axes adjacent to the thrusts. The modification of Antler-related fold orientations (north-south)

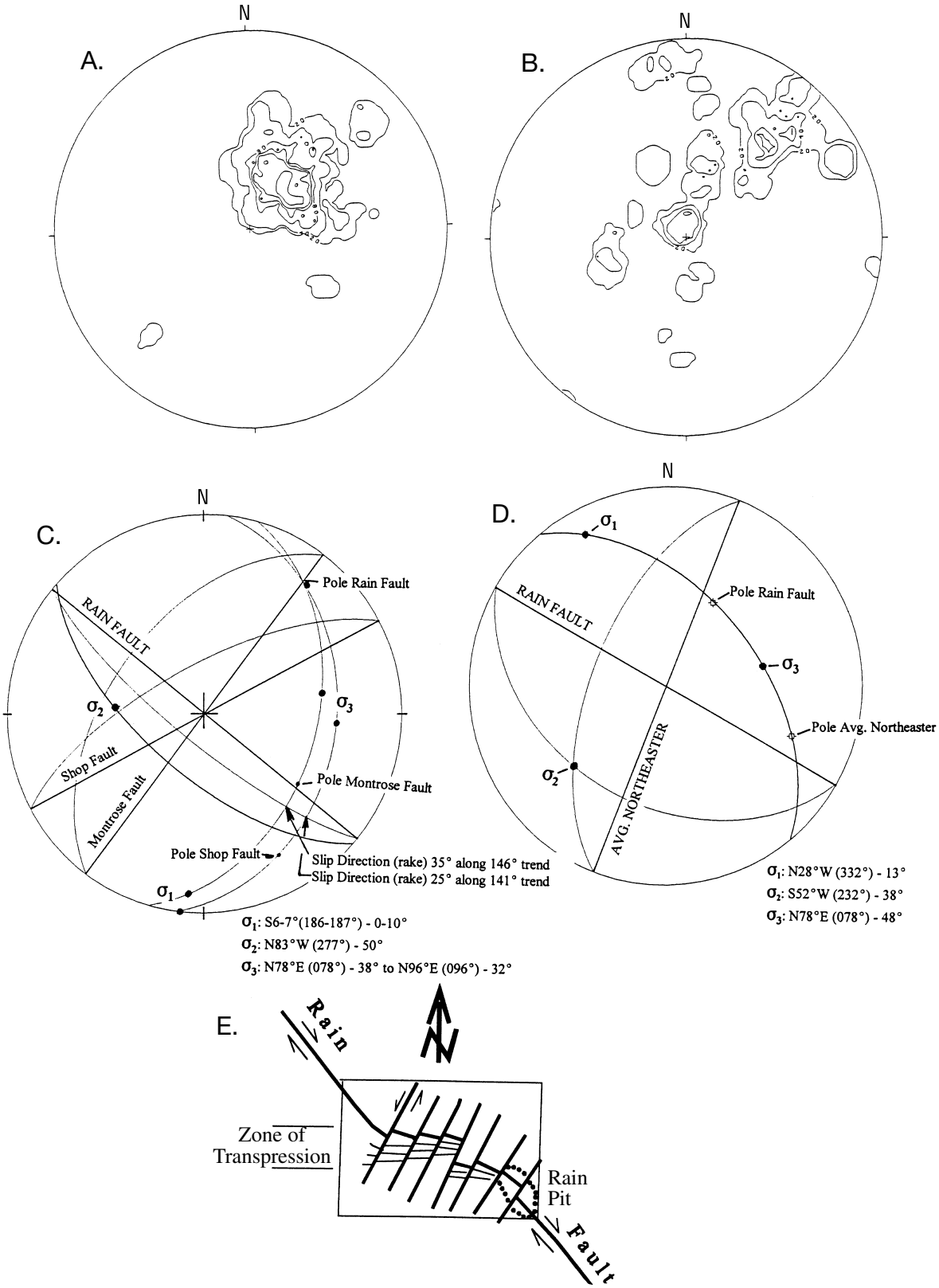


FIG. 6. Structural data from Rain mine. Stereonets are projections onto the lower hemisphere of Schmidt nets. A. Poles to bedding stereonet, hanging wall of Rain fault. B. Poles to bedding stereonet, footwall of Rain fault. C. Stress-field orientation from faults in the Rain open pit, showing predicted rakes on Rain fault. D. Stress-field orientations from faults in the Rain underground workings. E. Schematic map of faults in the Rain mine area, showing zone of transpression with associated flower faults.

by later tilting and shear-related rotation of fold axes to southwest or west trends is consistent with shear-related modification of the older folds.

The district-scale effect of the northeast set is a series of dominolike blocks dropped down to the northwest, with horsts and grabens formed locally by the antithetic set (Figs. 3 and 4). The geometry is similar to other domino-style fault arrays with both planar rotational faults and listric fault configurations, as described by Wernicke and Birchfiel (1982) and McClay and Ellis (1987). The structural style is commonly associated with extensional tectonics (Proffett, 1977; Gans et al., 1985). Postore displacement is interpreted to be associated with Basin and Range extension, regionally estimated at 64 to 100 percent (Wernicke and Birchfiel, 1982). The more easterly striking (N 20°–45° E) northeast-trending fault set geometries agree well with Basin and Range listric normal fault models proposed by Proffett (1977), Wernicke and Birchfiel (1982), and Gans et al. (1985).

### *Regional implications of an ore-controlling right-lateral fault event*

Transpressional right-lateral motion on the Rain fault system would have required northwest-southeast-directed compression. Nearly identical deformation with ore-controlling northwest-striking faults and folds has been documented south of Rain in the Alligator Ridge area (Nutt, 1997) and at South Bullion (Putnam and Henriques, 1991). At the Gold Quarry mine (23 km north of the Rain mine), the N 45° W striking Good Hope reverse fault and secondary northeast-striking faults localize that orebody (Rota, 1996). Cole (1995) documented strike-slip kinematic indicators on northwest- and northeast-striking faults in the pit area. Using those average strikes, stereonet solutions predict a principal stress direction of 20°, S 10° E at Gold Quarry, similar to the orientation predicted from the Rain mine fault data.

B. Putnam and D. McFarlane (written commun., 1990) suggested that the Carlin trend is controlled by a regional-scale N 45° W wrench fault system consisting of northwest-striking right-slip faults and northeast-striking left-slip faults. Shawe (1965) has recognized a similar wrench-fault fabric throughout Nevada. Strike-slip displacement on the Carlin trend may be an inboard manifestation of oblique collision of the North American and Pacific crustal plates beginning in the late Mesozoic and peaking in the Cenozoic (B. Putnam and D. McFarlane, written commun., 1990).

## Breccia and Mineral Paragenesis

### *Introduction*

The Rain orebody is hosted entirely within a relatively flat-lying breccia mass. In cross sections oriented northeast-southwest, perpendicular to the Rain fault, the breccia mass is a wedge-shaped body above the Devils Gate Limestone-Webb Formation contact. It is thickest adjacent to the Rain or Rain subparallel faults and adjacent to conjugate northeasterly faults (Fig. 3). The breccia mass is traceable for more than 5 km along the Rain fault. Four texturally distinct breccia types are recognized: (1) crackle breccia; (2) heterolithic, matrix-supported breccia; (3) tuffisite with accretionary lapilli; and (4) basal heterolithic breccia on the Devils Gate Limestone upper contact.

### *Crackle breccia*

Crackle breccia is characterized by dilatant fractures with matching walls (Fig. 7A), grading downward into fragment-supported breccia. The breccia typically contains more than 85 percent fragments, and the average interfragment to fragment ratio (I/F) is 5:95. The breccia is cemented by interfragment rock flour, fine fragments of Webb Formation rocks, barite, and quartz. Fragments are angular and delicate with little evidence of abrasion, rotation, or transport. Fragments commonly form a jigsaw-puzzle texture, where pieces can be fit back together. Crackle breccia ranges from 12 cm to 14 m thick as an irregular cap to the composite breccia mass, increasing in thickness where associated with prebreccia northwest- and northeast-striking faults.

The Webb Formation-crackle breccia contact is typically marked by a sharp contact between refractory and oxide ores, with the crackle breccia oxidized beneath as much as 350 m of overlying unoxidized, carbonaceous Webb and Chainman Formations. Drilling to the northwest beyond the current workings, however, shows that the crackle breccia becomes carbonaceous and sulfidic with increasing depth. The Webb Formation is intensely argillized within 14 m of the contact with the crackle breccia; this alteration is commonly fracture-controlled but locally pervasive. The matrix and margins of fragments in the crackle breccia exhibit weak to intense silica replacement, accompanied by 1 to 5 percent barite. Primary sedimentary textures in fragments are preserved. The crackle breccia contains some of the highest gold grades in the mine, locally exceeding 34 g/t. Higher grades are associated with more intense silica replacement. Like the oxide-refractory contact, the grade cutoff between crackle breccia and overlying argillized Webb Formation is extremely sharp, with changes from 34 g/t to less than 0.2 g/t over several centimeters.

### *Heterolithic, matrix-supported breccia*

The contact between the overlying crackle breccia and underlying heterolithic, matrix-supported breccia is invariably sharp and scoured, with local protrusions of the latter upward into the crackle breccia. Three brecciation events can be distinguished within the heterolithic, matrix-supported breccia. The products of these events, termed breccias A, B, and C, are described below and are also divided into oxidized and unoxidized varieties. The recognition of breccias A, B, and C comes primarily from Rain pit mapping by Williams (1992).

*Breccia A:* The first breccia event is now principally represented by blocks of breccia A within later breccia products (Williams, 1992). Breccia A comprises only 10 percent of the composite breccia mass and, where present as an intact breccia product, it occurs as relicts on the margin of the composite breccia mass. The breccia A blocks consist of matrix- to local fragment-supported heterolithic breccias with I/F values ranging from 12:88 to 35:65. Fragments are angular to rounded and less than 5 cm wide (Fig. 7B). Fragments include 30 to 80 percent silicified sedimentary rocks (locally including upward-transported Devils Gate Limestone), 40 to 90 percent vein material, 0 to 15 percent biotite-altered siltstone, 0 to 8 percent biotite vein fragments, and 0 to 9 percent pyrite vein fragments.

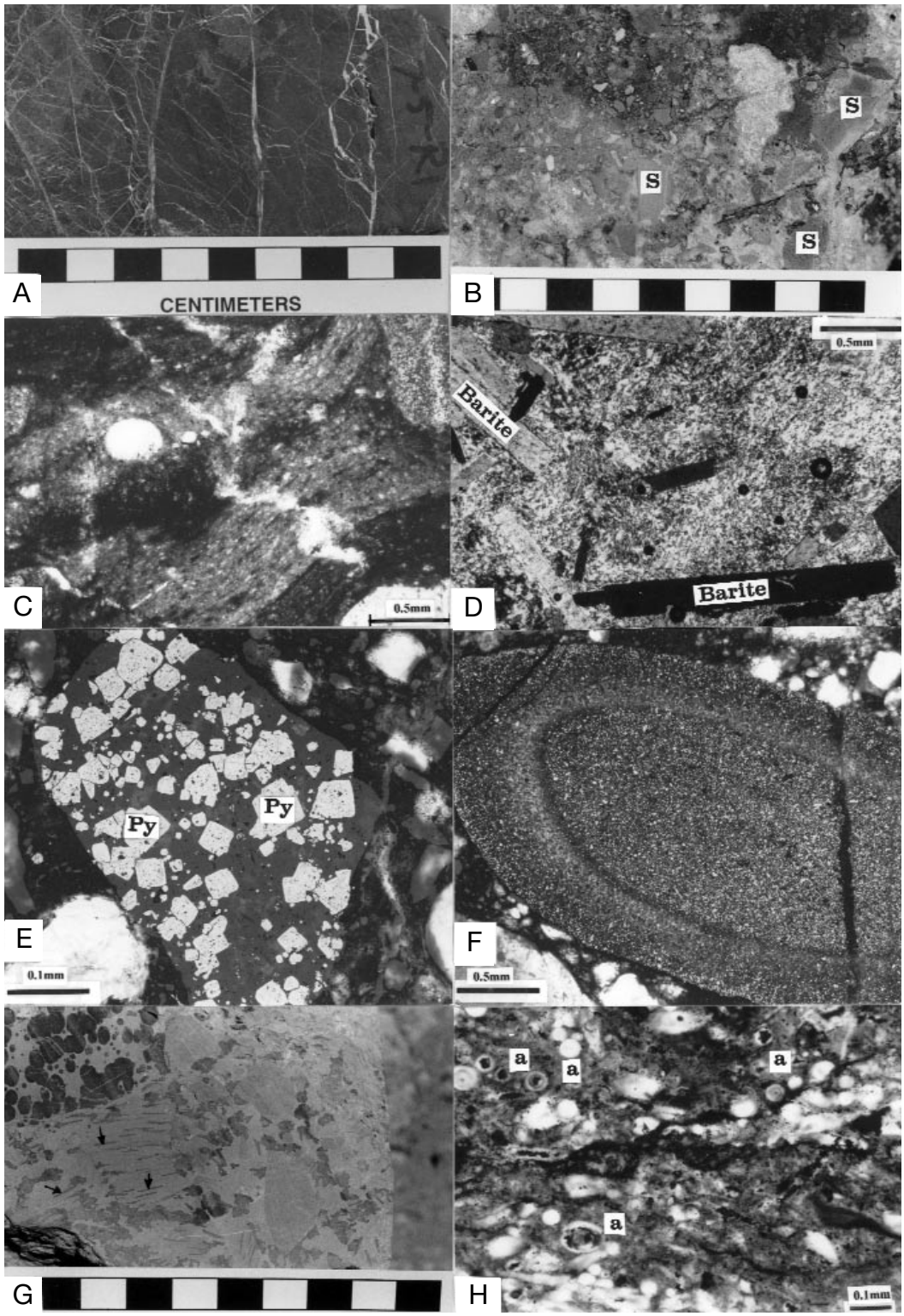


FIG. 7. Photographs of rocks from the Rain mine. A. Crackle breccia in carbonaceous Webb siltstone cemented by barite (white). B. Heterolithic matrix-supported hydrothermal breccia A from Rain pit adjacent to the Sharpstone fault; siltstone (s) and barite (white) fragments are in a weakly silicified rock flour matrix; scale is cm. C. Photomicrograph of flow-oriented fluidized matrix in breccia B around fragments and rounded quartz detritus, and cut by irregular barite veinlets (white). D. Photomicrograph of matrix barite euhedra and microcrystalline quartz matrix from hydrothermal breccia C stage. E. Photomicrograph of pyrite (Py)-quartz vein fragment in Rain hydrothermal breccia. F. Photomicrograph of pyritized hydrothermal breccia fragment with diffusion banding indicating pyrite introduction after breccia development. G. Accretionary lapilli (a) with slump flattening of lapilli (arrows) from tabular fluidized dikes in the Rain open pit; scale is cm. H. Photomicrograph of silicified accretionary lapilli (a) with multiple concentric bands in fluidized and fragment-aligned hydrothermal breccia.

Sedimentary rock fragments include weakly to intensely silicified sandstone, siltstone, mudstone, limestone, and conglomerate. Some fragments contain up to 8 percent introduced biotite in 2 mm-long grains encapsulating detrital quartz grains. Veinlets of biotite in silicified sedimentary rock fragments are locally present. The veinlets contain as much as 70 percent biotite encapsulating quartz (detrital and veinlet euhedra), sphalerite, and pyrite. Local barite (60–100%), euhedral quartz, pale green sphalerite (1–5%), euhedral pyrite (1–5%,) and traces of realgar in veinlets with grain sizes ranging from 1 to 5 mm cut the biotite veinlets and matrix of breccia A fragments. Locally these later sulfidic veins are dominantly pyrite (98%), with irregular sphalerite inclusions in the pyrite or as anhedral grains less than 1 mm long, and contain trace amounts of arsenopyrite and arsenian pyrite identified by X-ray and spectral analysis of pyrite grains. Pyrite veins with pyrite fragments in a pyrite cement have been observed (Williams, 1992). The sulfide veinlets do not extend out of breccia A blocks, indicating that they formed prior to subsequent breccia events.

Grains in the breccia A matrix are less than 1 mm in diameter and consist of rock flour with variable detrital and veinlet quartz, pyrite, biotite, barite, illite, organic carbon, iron oxides, and kaolinite. Breccia A is overprinted by silica flooding with distinctive reticulate texture containing traces of coprecipitated pyrite and sphalerite.

*Breccia B:* Intact breccia B constitutes about 20 percent of the composite breccia body and is common closer to the margins of the entire mass or in blocks throughout the later breccias. Matrix- to local fragment-supported breccias with I/F values ranging between 40:60 and 15:85 typify breccia B. Banding represented by generally steeply inclined tabular fragments with deflections of finer matrix around fragments (Fig. 7C) are characteristic. Fragments up to 6 cm in maximum size include 20 to 60 percent prebreccia silicified fragments, 20 to 80 percent early vein material from breccia A, and 10 to 50 percent other breccia A fragments. Breccia B matrix is rock flour with quartz euhedra fragments from breccia A, detrital quartz, pyrite, and barite. Oxidized portions of the breccia contain jarosite, dussertite, goethite, kaolinite, and alunite. Microcrystalline quartz floods and replaces matrix and fragment margins in breccia B.

*Breccia C:* Breccia C constitutes approximately 70 percent of the composite breccia mass and is the most well-developed along northwest- and northeast-trending faults. It is a matrix-supported, heterolithic breccia with I/F values ranging from 10:90 to 60:40. Fragments are angular to well rounded and less than 6 cm wide. Steep to nearly horizontal banding is common. Fragments include 20 to 70 percent breccia A veinlets, 20 to 60 percent prebreccia silicified sedimentary fragments, 10 to 40 percent breccia A, 10 to 40 percent breccia B, and 0 to 5 percent biotite vein fragments. The matrix is similar to that of breccia B. Unlike breccias A and B, however, breccia C is cemented with calcite inclusion-rich barite as laths and rosettes up to 9 mm long, or locally by microcrystalline hydrothermal quartz (Fig. 7D). Black barite is locally present as cement, with fine carbon fragments providing the color. Diagnostic properties of breccia C include coarse barite cement and breccia B fragments. Voids and fractures in breccia C are commonly filled with subhedral barite, drusy quartz, and later phosphate minerals including metavariscite, crandallite, and wavellite. Breccia C is also commonly cut by low-angle barite veins up to 1 m thick.

Pyrite occurs as fragments in all three breccia types. Additionally, some rocks and veinlets contained pyrite prior to being fragmented (Fig. 7E), whereas others had pyrite introduced after fragmentation (Fig. 7F), with pyrite bands subparallel to fragment margins.

*Tuffisite and accretionary lapilli*

Williams (1992) identified irregular bodies composed of clay-sized fragments containing accretionary lapilli that crosscut crackle and heterolithic, matrix-supported breccias in the Rain open pit, locally extending into the Webb Formation above the breccia. The zones occur as pipelike, dikelike, and sillike bodies with 40 to 80 percent lapilli in a rock flour matrix. The lapilli range from 1 mm to 1.2 cm in diameter. Thin section and X-ray diffraction (XRD) analyses indicate they are composed of rock flour particles (<0.05 to 0.5 mm; Fig. 7G, H) composed of 20 to 50 percent illite platelets less than 0.03 mm long, 30 to 50 percent quartz as angular to rounded fragments less than 0.05 mm in diameter, 5 to 15 percent barite as subangular to rounded fragments, 0 to 5 percent jarosite as pseudomorphs after pyrite fragments, 0 to 80 percent phosphates (metavariscite and crandallite) as local replacements of all other minerals, and traces of microcrystalline goethite, dussertite, kaolinite, and alunite (Williams, 1992). One of the better exposures in a bench face (now mined away) was a pipelike body 11 m wide cutting banded breccia C along a well-defined and scoured contact; the pipe contained early-stage consolidated accretionary lapilli breccia cut by pipelets of later, poorly consolidated accretionary lapilli in a rock flour matrix. The more consolidated portion of the pipe contained fragments or blocks with accretionary lapilli in rock flour matrix; the blocks were as much as 1 m wide. Accretionary lapilli in the blocks showed variable flattening (Fig. 7G). Such slumping is common in lapilli pipes due to periodic decreased fluid pressure and subsequent compaction (McCallum, 1985). Similar accretionary lapilli zones have been observed in core recovered from underground drill stations.

In the underground portion of the Rain mine, similar irregular to tabular, light gray, fine-grained clayey masses occur along northwest- and northeast-striking faults, as well as in irregular bodies through the heterolithic breccia. They commonly contain white spherical clay masses (accretionary lapilli) less than 1 mm in diameter. In some, the white clay has been removed, leaving small spherical cavities with a white rind of clay. Locally, these bodies have alternating light- and dark-colored layers composed of fine-grained rock flour (light colored) and sulfidic fragments (dark colored). The banding occurs along the margins of the bodies, whereas the medial portions, which have disseminated marcasite, have no apparent fragment orientation. Petrographic studies of these masses indicate they are composed entirely of fine fragmental material without any significant cement. As a result, the bodies are particularly unstable in underground exposures and require additional mine support. They are classified as tuffisites due to the interpreted process of their emplacement

as fluidized particulate material, locally with accretionary lapilli. The apparent increase in lapilli within tuffisite bodies at higher structural settings (i.e. to the southeast) compared to the underground workings, is interpreted to be the result of a higher degree of fluidization at shallower levels in the hydrothermal system.

*Basal heterolithic breccia*

The basal heterolithic breccia occurs as an irregular blanket, 0 to 60 m thick, along the top of the Devils Gate Limestone and extending upward in irregular contact with the heterolithic, matrix-supported breccia. The thickest zones are structurally controlled and commonly extend downward along faults cutting the limestone. Local voids within this breccia mass are as much as 18 m high. The breccia is fragment-supported with I/F values of 10:90 to 40:60. Fragments are derived principally from the overlying breccia, but at the upper Devils Gate Limestone contact, abundant dolomitized limestone fragments are present. The basal breccia matrix is invariably a red clay containing quartz, illite, and kaolinite with local jarosite, Fe, As, and Mn oxides, alunite, siderite, dolomite, calcite, and montmorillonite. The red clay is interpreted as a product of insoluble residues formed during pre-Webb Formation karsting that was localized along the upper part of the Devils Gate Limestone.

## Gold Mineralization

The age of gold introduction at Rain is not known. It predates the oldest supergene alunite age of 22 Ma (Odekirk, written commun.,1989) and postdates the late Paleozoic sedimentary host rock. Gold-bearing fluids were introduced along the Rain and northeast-trending fault sets (Fig. 5); those fluids spread laterally into the permeable hydrothermal breccias. The entire Rain composite breccia body contains gold grades exceeding 0.3 g/t. The high-grade (>5.1 g/t) ore mined in the underground operation, however, is localized along the upper portions of the composite breccia (Figs. 3 and 4).

During open pit mining, it was discovered that barite commonly constituted as much as 40 percent or more of the mined rock. To the northwest in the underground workings, the barite content decreases to less than 5 percent on average. There is an overall corresponding increase in average gold grades to the northwest in the underground workings (Fig. 5), indicating an antipathetic relationship to barite concentrations.

## Sulfur Isotopes

Williams (1992) reported sixteen sulfur isotopic analyses on hand-picked pyrite, barite, alunite, and jarosite from Rain pit samples (Fig. 8). Sulfate sulfur ratios from alunite and jarosite overlap the hydrothermal and diagenetic pyrite sulfur ratios, but barite sulfur ratios are significantly higher (Fig. 8). Field (1966) demonstrated that supergene sulfates derived their isotopic values, with no fractionation, directly from the sulfide sulfur that was oxidized during weathering. It is evident that alunite and jarosite at Rain formed during weathering of pyrite.

Potassium-argon dates on three alunite samples from the Rain pit range from 12.6 ± 0.5 Ma to 22.3 ± 0.9 Ma (J. Odekirk, written commun., 1989). A deeper level pit sample of alunite yielded a $^{40}Ar/^{39}Ar$ age of 20.7 ± 1.6 Ma (G. Arehart, written commun., 1991).

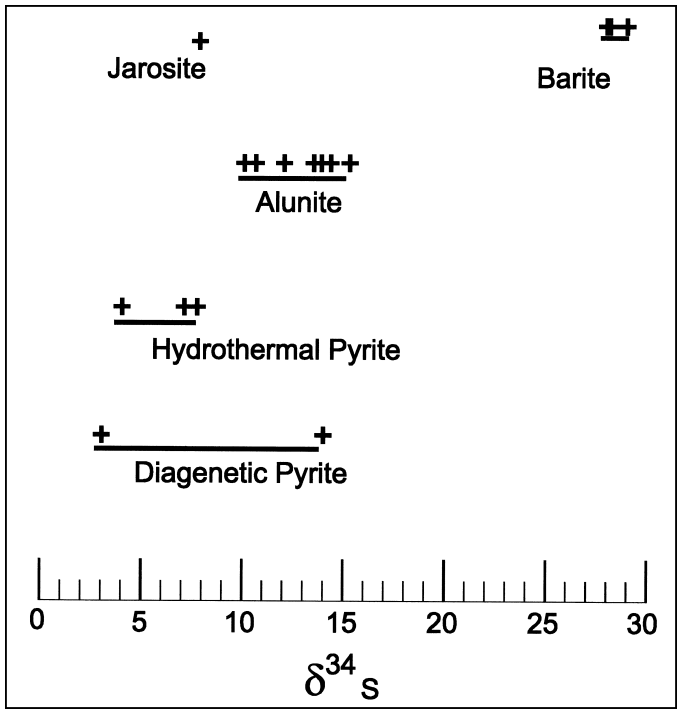


FIG. 8. Sulfur isotope ratios for diagenetic pyrite, hydrothermal pyrite, barite, and supergene alunite and jarosite from the Rain pit samples.

## Interpretation

A five-stage model for development of the Rain mine breccias and gold orebody is proposed. This model is based on detailed mapping, core logging, and petrographic studies of open pit and underground mine ores.

*Stage 1*

Stage 1 was related to the development of the Rain structural fabric associated with right-lateral oblique displacement (Fig. 9A) that enhanced the permeability of the Webb Formation immediately above the rheological boundary with the underlying Devils Gate Limestone. A series of faults, developed simultaneously subparallel to the Rain fault and with local changes westward in the strike, led to development of flower faults (Fig. 9A) that flatten outward (Fig. 3). The combination of right-lateral Rain fault displacement in conjunction with left-lateral offsets along the northeast-trending faults resulted in a significant increase in rock permeability at that lithologic boundary.

*Stage 2*

Stage 2 was initiated as hydrothermal fluids were introduced along the faults, generating early rock alteration (argillization, silicification, and pyrite-marcasite formation), fragmenting the clastic rocks, and forming hydrothermal crackle and fluidized breccia masses during multiple events (Fig. 9B). Textures attributable to fluidization at Rain include well-rounded breccia fragments, abundant rock flour matrix

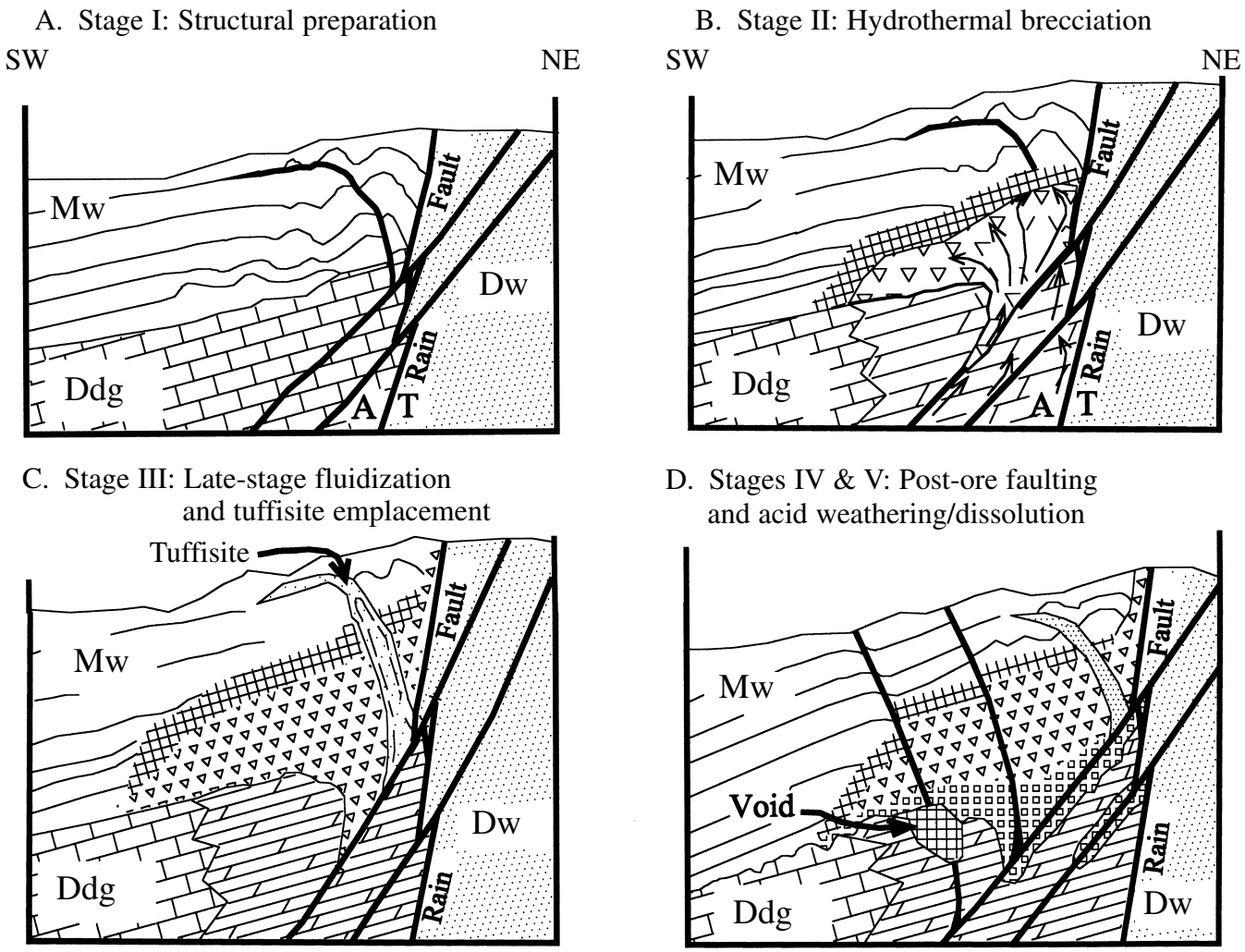


FIG. 9. Diagrammatic southwest-northeast cross sections of the Rain pit area illustrating the evolution of the Rain mine faults and breccias (Mw = Webb Formation; Ddg = Devils Gate Limestone; Dw = Woodruff Formation). A. Structural preparation adjacent to the Rain right-oblique fault (T= toward viewer and A= away from the viewer) and subparallel fault, showing their offset by northeast-striking structures that are subparallel to the plane of the section; Rain subparallel faults flatten outward, forming a flower structure (see Fig. 3 for a true crosssection). B. Introduction of hydrothermal fluids with initiation of hydrothermal breccia formation exhibiting a transition through crackle breccia (cross-hatch pattern) into overlying Webb siltstones; wall-rock alteration and gold introduction occurred during this stage. C. Late-stage fluidization along faults forming tuffisite dikes, locally containing accretionary lapilli, crosscutting hydrothermal breccia (triangle-symbol pattern). D. Postore offsets of breccia and orebody occur along northeast-striking extensional, antithetic faults (shown diagrammatically merging with earlier northeast-striking faults that offset the Rain fault); oxidation of sulfides accompanies downward percolation of acid groundwater, which also argillizes the breccias near the floor of the breccia mass, dissolves carbonates, and forms collapse breccias (square-symbol pattern) replaced by clays and alunite with local cavern development.

locally exhibiting flow orientation (Fig. 7C), and thorough mixing of fragment types derived from above and below the position of the observed breccia. The breccia appears to have extended upward along the Rain fault, and it clearly extended laterally along the Webb-Devils Gate contact as well. This lateral breccia extension may have been the result of lower permeability upward into the Webb Formation due to formation of the clay alteration capping over the crackle breccia zone, forcing doming of the overlying rocks and lateral fluid flow within the strongly broken and argillized contact zone. The Devils Gate Limestone adjacent to the northwest- and northeast-trending faults was dolomitized. Gold was deposited in the late stages of breccia formation with the pyrite-marcasite deposition, primarily in arsenian rims on marcasite.

*Stage 3*

Stage 3 represents the late stage of hydrothermal activity during which time the discordant tuffisite dikes with local accretionary lapilli formed, principally along narrow fault-localized conduits (Fig. 9C). Although these are locally mineralized, they appear to have been emplaced late in the hydrothermal cycle, possibly deriving their gold content from the rocks through which they were emplaced. We interpret that the Rain hydrothermal system did not freely vent to the

paleosurface and thus retained a high proportion of the rock flour generated during fluidized brecciation. Accretionary lapilli form when fluids vent through cohesive clay-sized material (McCallum, 1985) by accretion of electrostatically charged fine sand and clay particles to a central grain and each other (Woolsey, 1973; McCallum, 1985; Baker et al., 1986). Lapilli at Rain are dominated by tangentially arranged, highly chargeable clay particles, whereas matrix material is relatively enriched in slightly coarser barite, pyrite, and quartz grains. The lapilli were suspended by fluid streaming and grew by progressive enlargement during agitation and rotation (Woolsey, 1973; McCallum, 1985). Based on experimental studies, Woolsey (1973) noted that blocks from the walls of lapilli pipes were pulled into the conduit during continued fluidization. Slumping of material into conduits also resulted from compaction during phases of decreased gas pressure. This process could explain the slumping and rotated blocks of lapilli breccias and sheared lapilli (Fig. 7G) observed in the Rain pit.

*Stage 4*

Stage 4 was related to postore normal faulting, resulting in offsets of the Rain orebody (Figs. 3 and 9D). The faults are northeast striking and they are associated with Basin and Range extension. The originally flat-lying Rain mineralized hydrothermal breccia complex was bisected by normal offset on northeast-trending faults and parasitic reactivation of earlier-formed north-northeast-striking structures. The net effect was a series of rotated blocks dropped down to the northwest with local horsts and grabens developed by antithetic structures (Figs. 3 and 9D). In the absence of depth control, we interpret that the northeast-striking fault geometries are similar to those described by Proffett (1977), Wernicke and Burchfiel (1982), and Gans et al. (1985; Fig. 3), with local antithetic structures (Fig. 9D) that merge with the extensional structures. A precise age for Basin and Range faulting in the Rain area is unknown, but supergene alunite ages as old as 22 Ma indicate that extension and weathering had begun at that time. Therefore, stage 4 is interpreted to be the effect of Basin and Range extensional tectonism.

*Stage 5*

Stage 5 was the formation of collapse breccias along the upper surface of the Devils Gate Limestone during supergene oxidation and alteration (Fig. 9D). Sulfide oxidation (weathering) generated acidic solutions that moved downward to the Devils Gate Limestone where extensive dissolution occurred. Collapse of the overlying hydrothermal breccia complex into the open spaces occurred concomitantly; however, some large cavities were not infilled by collapse.

## Acknowledgments

Reviews of earlier drafts by Sam Romberger, Jean Cline, Eric Seedorff, and Marco Einaudi contributed to an improved manuscript. We acknowledge the many contributions made by Newmont exploration and mine geologists. Newmont management supported the research and gave permission to publish these results. The Ralph J. Roberts Center for Research in Economic Geology (CREG) at Mackay School of Mines, the University of Nevada, Reno provided support for part of this research. Sulfur isotope analyses were performed by Geochron Laboratories, Cambridge, Massachusetts.

*April 27, 1998; October 1, 1999*

## REFERENCES

Arehart, G.B., Foland, K.A., Naeser, C.W., and Kesler, S.E., 1993, $^{40}Ar/^{39}Ar$ and fission track geochronology of sediment-hosted disseminated gold deposits at Post-Betze, Carlin trend, northeastern Nevada: Economic Geology, v. 88, p. 622–646.

Baker, E.M., Kirwin, D.J., and Taylor, R.G., 1986, Hydrothermal breccia pipes: James Cook University of North Queensland Economic Geology Research Unit, Contribution 12, 35 p.

Christensen, O.D., 1993, Carlin trend geologic overview: Society of Economic Geologists Field Trip Guidebook, v. 18, p. 12–26.

Cole, D.M., 1995, Structural evolution of the Gold Quarry deposit and implications for development, Eureka County, Nevada: Unpublished M.S. thesis, Fort Collins, Colorado State University, 79 p.

Emsbo, P., Hofstra, A., Zimmerman, J.M., and Snee, L., 1996, A mid-Tertiary age constraint on alteration and mineralization in igneous dikes on the Goldstrike property, Carlin trend, Nevada [abs.]: Geological Society of Nevada Newsletter, November 1996, p. 3.

Evans, J.G., 1980, Geology of the Rodeo Creek NE and Welches Canyon quadrangles, Eureka County, Nevada: U.S. Geological Survey Professional Paper 1473, 81 p.

Field, C.W., 1966, Sulfur isotopic method for discrimination between sulfates of hypogene and supergene origin: Economic Geology, v. 61, p. 1478–1485.

Gans, P.B., Miller, E.L, McCarthy, J., and Ouldcott, M.L., 1985, Tertiary extensional faulting and evolving ductile-brittle transition zones in the northern Snake Range and vicinity: New insights from seismic data: Geology, v. 13, p. 189–193.

Hodgson, C.J., 1989, The structure of shear-related, vein-type gold deposits: A review: Ore Geology Reviews, v. 4, p. 231–273.

Knutsen, G.C., and West, P.W., 1984, Geology of the Rain disseminated gold deposit, Elko County, Nevada: Arizona Geological Society Digest, v. 15, p. 73–76.

Maher, B., 1997, Mississippian sedimentary rock-hosted gold deposits of the eastern Great Basin: Relative importance of stratigraphic and structural ore controls: Society of Economic Geologists Guidebook Series, v. 28, p.171–182.

McCallum, M.E., 1985, Experimental evidence for fluidization processes in breccia pipe formation: Economic Geology, v. 80, p. 1523–1543.

McClay, K.R., and Ellis, P.G., 1987, Geometries of extensional fault systems developed in model experiments: Geology, v. 15, p. 341–344.

Nutt, C.J., 1997, Sequence of deformational events and the recognition of Eocene(?) deformation in the Alligator Ridge area, east-central Nevada: Society of Economic Geologists Guidebook Series, v. 28, p. 203–211.

Proffett, J.M., Jr., 1977, Cenozoic geology of the Yerington district, Nevada, and implications for the nature and origin of Basin and Range faulting: Geological Society of America Bulletin, v. 88, p. 247–266.

Putnam, B.R., III, and Henriques, E.Q.B., 1991, Geology and mineralization at the South Bullion deposit, Pinon Range, Elko County, Nevada, *in* Raines, G.L., Lisle, R.E., Schafer, R.W., and Wilkinson, W.H., eds., Geology and ore deposits of the Great Basin: Geological Society of Nevada Symposium, Reno, April 1–5, 1990, Proceedings p. 713– 729.

Rota, J.C., 1996, Gold Quarry: A geologic update, *in* Green, S.M., and Struhsacker, E., eds., Geology and ore deposits of the American cordillera: Geological Society of Nevada Field Trip Guidebook Compendium, 1995, Reno/Sparks, p. 157–166.

Shawe, D.R., 1965, Strike-slip control of Basin-Range structure indicated by historical faults in western Nevada: Geological Society of America Bulletin, v. 76, p. 1361–1378.

Smith, J.F., and Ketner, K.B., 1968, Devonian and Mississippian rocks and the date of the Roberts Mountains thrust in the Carlin-Piñon Range area, Nevada: U.S. Geological Survey Bulletin 1251-I, 18 p.

——1975, Stratigraphy of Paleozoic rocks in the Carlin-Piñon Range area: U.S. Geological Survey Professional Paper 867-A, 87 p.

Stewart, J.H., 1980, Geology of Nevada: Nevada Bureau of Mines and Geology Special Publication 4, 136 p.

Sylvester, A.G., 1988, Strike-slip faults: Geological Society of America Bulletin, v. 100, p. 1666–1703.

Teal, L., and Jackson, M., 1997, Geologic overview of the Carlin trend gold deposits and descriptions of recent deep discoveries: Society of Economic Geologists Guidebook Series, v. 28, p. 3–37.
Wernicke, B., and Burchfiel, B.C., 1982, Modes of extensional tectonics: Journal of Structural Geology, v. 4, p. 105–115.
Wilcox, R.E., Harding, T.P., and Seely, D.R., 1973, Basic wrench tectonics: American Association of Petroleum Geologists Bulletin, v. 57, p. 74–96.
Williams, C.L., 1992, Breccia bodies in the Carlin trend, Elko and Eureka Counties, Nevada: Classification, interpretation, and roles in ore formation: Unpublished M.S. thesis, Fort Collins, Colorado State University, 213 p.
Woolsey, T.S., 1973, Physical modeling of diatreme emplacement: Unpublished M.S. thesis, Fort Collins, Colorado State University 92 p.